J Mater Sci: Mater Med (2011) 22:2119–2130
DOI 10.1007/s10856-011-4387-3

Precision microchannel scaffolds for central and peripheral nervous system repair

Daniel Lynam · Bridget Bednark · Chelsea Peterson · David Welker · Mingyong Gao · Jeffrey S. Sakamoto

Received: 9 February 2011 / Accepted: 30 June 2011 / Published online: 16 July 2011

Abstract In previous studies, we demonstrated the ability to linearly guide axonal regeneration using scaffolds comprised of precision microchannels 2 mm in length. In this work, we report our efforts to augment the manufacturing process to achieve clinically relevant scaffold dimensions in the centimeter-scale range. By selective etching of multi-component fiber bundles, agarose hydrogel scaffolds with highly ordered, close-packed arrays of microchannels, ranging from 172 to 320 μm, were fabricated with overall dimensions approaching clinically relevant length scales. Cross-sectional analyses determined that the maximum microchannel volume per unit volume of scaffold approached 80%, which is nearly twice that compared to our previously reported study. Statistical analyses at various points along the length of the microchannels also show a significant degree of linearity along the entire length of the scaffold. Two types of multi-component fiber bundle templates were evaluated; polystyrene and poly(methyl methacrylate). The scaffolds consisting of 2 cm long microchannels were fabricated with the poly(methyl methacrylate) fiber-cores exhibited a higher degree of linearity compared to those fabricated using polystyrene fibers. It is believed that the materials process developed in this study is useful for fabricating high aspect ratio microchannels in biocompatible materials with a wide range of geometries for guiding nerve regeneration.

D. Lynam · B. Bednark · C. Peterson · J. S. Sakamoto (✉)
Department of Chemical Engineering and Materials Science, Michigan State University, College of Engineering, East Lansing, MI 48824, USA
e-mail: jsakamot@msu.edu

D. Welker
Paradigm Optics, Inc, Vancouver, WA 98682, USA

M. Gao
Department of Neuroscience, University of California, San Diego, La Jolla, CA 92093, USA

1 Introduction

Spinal cord and peripheral nerve injuries are debilitating and typically result in loss of function. It has been reported that approximately 1.9% of the US population in 2004 lived with some form of paralysis [1]. Although significant progress has been made in biomedicine within the past few decades, the cure for these injuries remains a challenge. Recent attempts at repairing peripheral nerve and spinal cord injuries have incorporated nerve guidance scaffolds (NGS) to direct axon regeneration [2–8]. Previously, repair of nerve injuries were attempted using auto- or allografts [9–11]. More recently, biosynthetic scaffolds have been used and are preferred to grafts because of the complications with obtaining and employing them, including (1) a need for separate tissue harvesting and thus increased surgeries, (2) receiver complications from immune system rejection, and (3) limited availability [12]. For a biosynthetic scaffold to be considered for in vivo testing, especially in the central nervous system (CNS), it must be compatible with the native nerve environment and therefore chemically inert. The biosynthetic scaffold must also possess a significant density or volume fraction of nerve guidance channels spanning the length of the implant or lesion site to ensure a high density of linearly oriented axons [13, 14].

Recent efforts involving templated agarose hydrogel scaffolds using highly ordered fiber arrays have demonstrated the ability to precisely promote and guide nerves in

the central nervous system [15, 16]. Briefly, this process uses the selective etching of optical fiber bundles to produce ordered arrays of semi-cylindrical pores with nerve guidance channel volume in the 44% range. When permeated with the appropriate neurotrophic factors and implanted in female rats, the scaffolds enable precise, linear axonal regeneration. The dimensions were 2.0 mm long, 1.5 mm in width and 1.3 mm deep. Although the nerve guidance has been achieved in the small mammalian model, the ultimate goal of this work is to develop a technology capable of repairing peripheral nerve and spinal cord injuries in humans. Work in other laboratories have used scaffolds approaching 1 cm as the target length in peripheral nerve repair and likewise is used in this work [17–21]. Additionally, target lengths for CNS repair have been established for 2 cm [4]. With the understanding that the length and geometry of each nerve injury will be unique amongst individual cases, our overall goal is to develop a robust patterning process capable of tailoring scaffold micro, meso and macro dimensions to accommodate the needs of each instance. To this end, the study reported herein describes the steps for augmenting the scaffold patterning process to enable the fabrication of scaffolds with clinically relevant dimensions. Specifically, the technological issues to be addressed are: (i) can scaffolds be fabricated with the same close-packed arrays of channels but at lengths compatible with human injuries? (ii) are the channels continuous at lengths approaching or greater than 1 cm? and (iii) can the cross-sectional dimensions of the scaffolds approach or exceed 1 cm^2?

As with our past study, agarose hydrogel was selected as the NGS material due to its biocompatibility with the central nervous system both chemically and mechanically. Agarose hydrogel has been shown to be compatible with our scaffold fabrication process and is strong enough to withstand the rigors of surgical implantation, maintain integrity in vivo, and remain soft enough to limit an immunoresponse [15]. Still, research has yet to demonstrate how effective agarose hydrogel scaffolds with clinically relevant dimensions are at guiding nerve growth. Likewise, related work has demonstrated that agarose hydrogel scaffolds could be implemented for sustained nerve growth factor release through the layer-by-layer (LbL) process to encourage growth of nerve axons along the length of the implant [22].

2 Materials and methods

2.1 Materials

Multi-component fiber bundles (MCFB) were fabricated by Paradigm Optics Inc. and consisted of various diameter cores surrounded by a continuous matrix. Two types of MCFBs were fabricated: one consisting of polystyrene (PS) fibers surrounded by a continuous matrix of poly(methyl methacrylate) (PMMA) (Fig. 1a), and another composed of PMMA fibers surrounded by a continuous matrix of PS, termed inverse MCFB (Fig. 1b). The solvents used to selectively etch the various fiber bundle constituents were propylene carbonate (PC) purchased from Sigma Aldrich, acetonitrile (ACN) and tetrahydrofuran (THF) from Mallinckrodt Baker and cyclohexane from Burdick and Jackson. The PS endcaps were cut from PS petri dishes purchased from VWR, while the PMMA endcaps were made from PMMA sheets purchased from McMaster-Carr. Hydrogel scaffolds were fabricated using distilled water and high molecular weight agarose (Type I-A, Low EEO, A0169) purchased from Sigma Aldrich. Agarose hydrogel potting solutions were made using low molecular weight agarose (Type XI, Low Gelling Temperature, A3038) purchased from Sigma Aldrich.

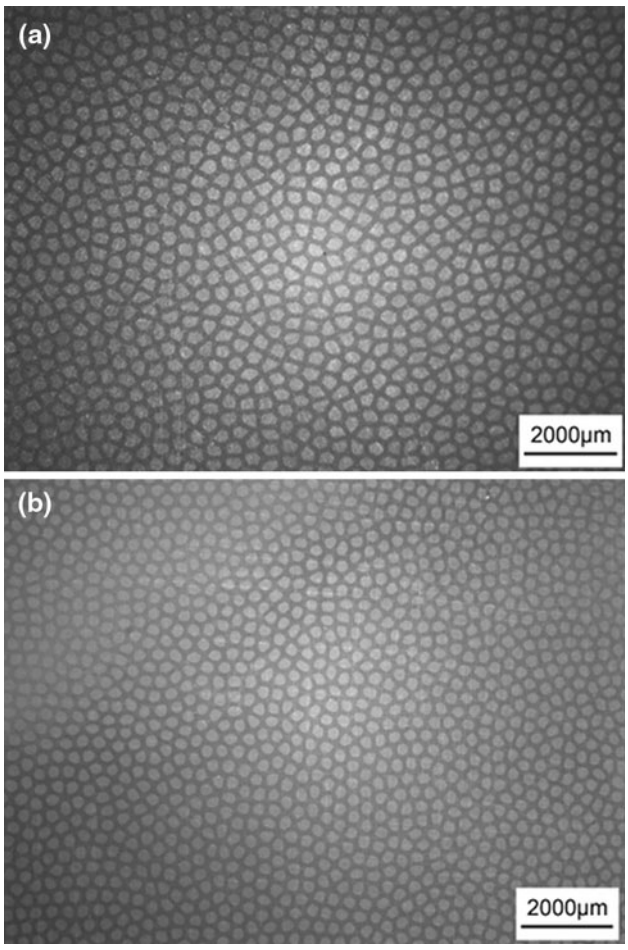

Fig. 1 As-received cross-sections of **a** polystyrene fiber, poly(methyl methacrylate) cladding MCFB and **b** inverse MCFB with PMMA fibers and PS cladding

2.2 Scaffold fabrication

The MCFB used to fabricate the majority of nerve guidance scaffolds in this study consisted of PS fiber cores surrounded by a continuous matrix of PMMA with a typical, as received length of 100 mm in the longitudinal direction. Typical MCFB cross-sections were square or rectangular ranging from 5 to 20 mm on one side. The range of PS fiber core diameters and spacing between cores is listed in Table 1. NGS templates were made by cutting MCFBs with a precision diamond saw to a desired length, squared and finished with 600 grit sandpaper, and rinsed with ethanol (Fig. 2a). PS rectangles with dimensions matching the MCFB template were cut from 1.0 mm thick sheets of PS and bonded to the finished ends of the template (Fig. 2b). Bonding was achieved by immersing the PS rectangles in cyclohexane at 45°C for 10 s and quickly pressing (approximately 50 psi) onto the ends of the cut template. PS rectangles were bonded to each of the MCFB ends this way. Cyclohexane was specifically chosen to selectively and partially dissolve only the PS fibers and the PS rectangles while maintaining the PMMA matrix intact. The same process was used to bond PS side supports spanning between polystyrene end caps, which gave the templates rigidity in the latter steps of processing (Fig. 2c). After curing of bonded PS, the template assemblies were immersed in a PC and ACN solvent bath (80/20 v/v, respectively) at 45°C and stirred with a magnetic stir bar at approximately 100 revolutions per minute for 24 h (Fig. 2d). Approximately 100 ml of etch bath was used per cubic centimeter of MCFB template. Since PS is not soluble in PC, the continuous PMMA matrix was selectively removed leaving only the PS fibers, end caps and side supports intact. After full PMMA removal, rinsing of the fiber template three times in distilled water for 15 min each followed by ethanol ensured complete removal of residual PMMA monomers. The fiber templates were then immersed in a 3/97 (w/w) agarose/distilled water solution at 85°C (Fig. 2e). Immediately following, centrifugation at 1000 rpm for 1 min was completed. Centrifugation facilitates molten agarose hydrogel permeation through the template. The template and molten agarose hydrogel was poured onto a flat surface of Teflon® and the open faces of the template were compressed between two plates during cooling. Compression on the template open faces ensured that no fibers stray outside the region confined by the PS end caps and side supports. Selective removal of the PS template components was achieved by immersing the agarose hydrogel-permeated template in a 99% THF bath (Fig. 2f) at room temperature for 24 h or until complete PS dissolution. Approximately 100 ml of THF was used per cubic centimeter of template. Additional THF baths were used if complete PS removal was not evident. The agarose hydrogel scaffolds were then rinsed in an ethanol bath, followed by triple rinsing with distilled water to remove residual solvents (Fig. 2g).

Nerve guidance scaffolds were also fabricated using inverse MCFB. The procedure is similar to the PS fiber/PMMA cladding MCFB scaffold fabrication process. Briefly, rectangular end caps with dimensions matching the inverse MCFB template were cut from 1.0 mm thick sheets of PMMA and bonded to the finished ends of the template. Bonding of end caps was achieved by immersing them in an 80/20 (v/v) mixture of PC and ACN, respectively, at 45°C for 60 s followed by compression (approximately 50 psi) onto the template ends. PMMA side supports were bonded this way. After curing of bonded PMMA, the template assemblies were immersed in cyclohexane at 45°C and stirred with a magnetic stir bar at approximately 100 revolutions per minute for 24 h. Because of its solubility in cyclohexane, the PMMA fibers, end caps, and side supports remain while the polystyrene matrix selectively dissolves. The remainder of the nerve guidance scaffold fabrication process is as previously explained.

2.3 Cross-sectional microchannel diameter and wall thickness at various depths

Scaffold cross-sectional analysis was conducted to characterize features such as the microchannel and wall dimensions and to determine the microchannel vol% per unit volume scaffold. MCFB template cross-sections were analyzed in a similar manner for comparison to scaffold measurements. For this study, scaffolds were prepared as described above but incorporated 0.02 vol% carbon black into the scaffold walls to improve contrast for optical imaging. The scaffolds were then immersed in molten 3 wt% low molecular weight agarose potting solutions at 60°C and centrifuged at 500 rpm for 1 min. Centrifugation permeated the low molecular weight agarose hydrogel through the scaffold microchannels. After cooling and gelation, the mounted scaffolds were rigid enough to withstand mechanical sectioning. Microchannel wall integrity was determined by depth analysis, which involved sanding 7.5 mm long scaffolds to depths of 1, 3.75, and 6 mm along the longitudinal axis. Lapping down to various depths was achieved using sandpaper (240 grit) and polished using fine (600 grit) sandpaper. Optical microscopy was performed on the sectioned scaffolds, which were viewed in transmission using fluorescent white light.

2.4 Scaffold porosity

The scaffold theoretical microchannel area or volume was both measured and also estimated based on cubic

Table 1 Scaffold characterization along the longitudinal axis and template cross-sectional analysis

	25/200 (W/MC = 0.125)						**43/320 (W/MC = 0.134)**					
	Scaffold depth analysis				Template cross-sectional	Percent difference	Scaffold depth analysis				Template cross-sectional	Percent difference
Depth	1 mm	3.75 mm	6 mm	Average	Average	Template/Scaffold	1 mm	3.75 mm	6 mm	Average	Average	Template/Scaffold
Wall Thickness (avg, μm)	27 ± 11	20 ± 2.1	27 ± 10	24.7 ± 8.7	27 ± 4	9.31	43 ± 7.8	38 ± 16	49 ± 16.4	43.3 ± 13.9	45 ± 8	3.93
Channel Diameter (avg, μm)	200 ± 5	200 ± 9.6	200 ± 7.1	200 ± 7.5	215 ± 9	7.50	317 ± 10.5	320 ± 2.7	323 ± 8.2	320 ± 7.8	332 ± 11	3.69
Area of Pore (avg, mm^2)	0.0364 ± 0.0005	0.0366 ± 0.0064	0.0362 ± 0.0043	0.0364 ± 0.0045	0.0382 ± 0.0032	4.95	0.07891 ± 0.0052	0.08063 ± 0.0043	0.08208 ± 0.0042	0.08054 ± 0.0046	0.0914 ± 0.0062	13.48
Channel Count per mm^2 (avg)	16.5				20.16	22.18	9.9				8.05	18.69
	54/172 (W/MC = 0.314)						**67/200 (W/MC = 0.335)**					
	Scaffold depth analysis				Template cross-sectional	Percent difference	Scaffold depth analysis				Template cross-sectional	Percent difference
Depth	1 mm	3.75 mm	6 mm	Average	Average	Template/Scaffold	1 mm	3.75 mm	6 mm	Average	Average	Template/Scaffold
Wall Thickness (avg, μm)	54 ± 11.1	52 ± 17.5	56 ± 12	54.1 ± 13.8	53 ± 8	2.03	67 ± 4.7	66 ± 3.1	67 ± 1.2	66.7 ± 3.3	54 ± 4	19.40
Channel Diameter (avg, μm)	178 ± 6.1	168 ± 1.9	171 ± 6.9	172.3 ± 5.4	166 ± 8	3.69	201 ± 6.6	199 ± 9.9	201 ± 7.2	200.3 ± 8	176 ± 10	12.00
Area of Pore (avg, mm^2)	0.0249 ± 0.0017	0.0221 ± 0.0002	0.023 ± 0.0018	0.0233 ± 0.0014	0.0229 ± 0.0024	1.72	0.0325 ± 0.0051	0.0336 ± 0.0055	0.0327 ± 0.0027	0.0329 ± 0.0046	0.0255 ± 0.0028	22.49
Channel Count per mm^2 (avg)	28.3				28.35	0.18	15.2				25.24	66.05
	88/210 (W/MC = 0.419)						***94/254 (W/MC = 0.370)**					
	Scaffold depth analysis				Template cross-sectional	Percent difference	Scaffold depth analysis				Template cross-sectional	Percent difference
Depth	1 mm	3.75 mm	6 mm	Average	Average	Template/Scaffold	1 mm	3.75 mm	6 mm	Average	Average	Template/Scaffold
Wall Thickness (avg, μm)	83 ± 8	87 ± 11.6	93 ± 4.9	87.7 ± 8.6	107 ± 19	22.01	108 ± 18.2	85 ± 16.9	90 ± 19.1	94.3 ± 18.1	104 ± 14	10.17
Channel Diameter (avg, μm)	214 ± 8.1	212 ± 5.9	204 ± 8.3	210.1 ± 7.5	240 ± 13	14.23	254 ± 19.5	253 ± 20	255 ± 18.4	253.8 ± 19.3	243 ± 12	4.26
Area of Pore (avg, mm^2)	0.0308 ± 0.0029	0.031 ± 0.0032	0.032 ± 0.0042	0.0313 ± 0.0035	0.0479 ± 0.0049	53.04	0.051 ± 0.0079	0.050 ± 0.0082	0.051 ± 0.0074	0.0507 ± 0.0078	0.0489 ± 0.0046	4.12
Channel Count per mm^2 (avg)	12.5				9.09	27.28	8.3				9.69	16.75

* inverse template

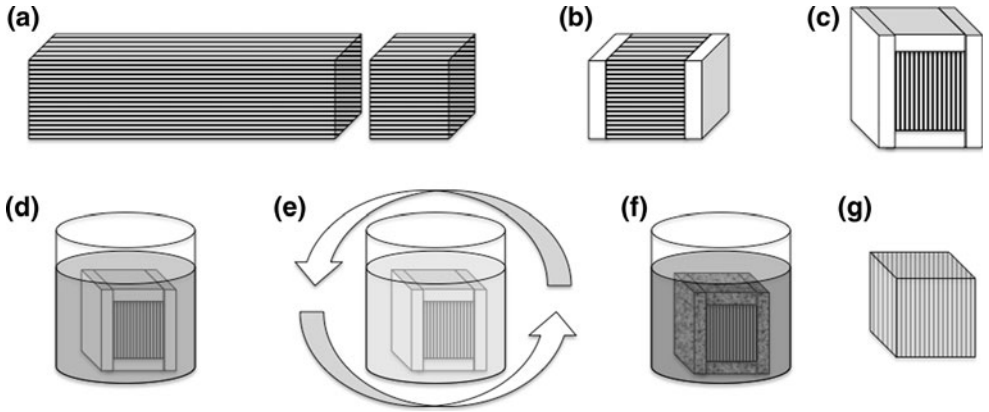

Fig. 2 MCFB scaffold fabrication showing **a** template sectioning, **b** end-cap bonding, **c** side support bonding, **d** cladding removal, **e** agarose hydrogel permeation by centrifugation, **f** fiber, end-cap, and side support dissolution, and **g** a finished agarose-based nerve scaffold

close-packed (CCP) arrays of cylinders and hexagonally close-packed (HCP) arrays of hexagons, as seen in Fig. 3. Briefly, the actual microchannel geometries are neither pure cylinders nor hexagons, but rather a mosaic of shapes. Thus, the observed open microchannel area should fall between a minimum value for cylinders packed in a CCP array and a maximum for hexagons in an HCP array. For cylindrical microchannels, the value R is defined as the radius of the microchannel, and the value G is the specified wall thickness. Similarly, for hexagonal microchannels, the width of the microchannel W is defined as the specified microchannel diameter and G is the specified wall thickness. If perfect cylinders in a CCP arrangement are observed, the unit cell or smallest repeating unit is confined to a square region enveloping two circular microchannels and diagonal of twice the gap width plus twice the diameter of the microchannel. Similarly, if perfect hexagons in a HCP arrangement are observed, the unit cell is confined to a hexagonal region enveloping one microchannel and a matrix width of half the wall thickness. Using the equations in Fig. 3, comparisons of pore area can be made between cylindrical microchannels in CCP arrangement (Eq. 1) and hexagons in HCP arrangement (Eq. 2).

The actual scaffold porosity was calculated by measuring 18 microchannels per scaffold across their lateral and longitudinal axes and taking the average value. A similar process was followed for determining average wall thickness. Subsequently, the area per microchannel was calculated by determining the pore area for each of the eighteen microchannels assuming them to be perfect hexagons or circles. The average of these values was taken as the actual area per microchannel. Summing the number of microchannels on a scaffold face and dividing by the total area determined the number of microchannels per mm^2. By multiplying the microchannel count and the actual pore area, the area fraction occupied by pores was determined.

3 Results and discussion

The goal of this study is to establish a technology to precisely guide axonal regeneration and ultimately provide a

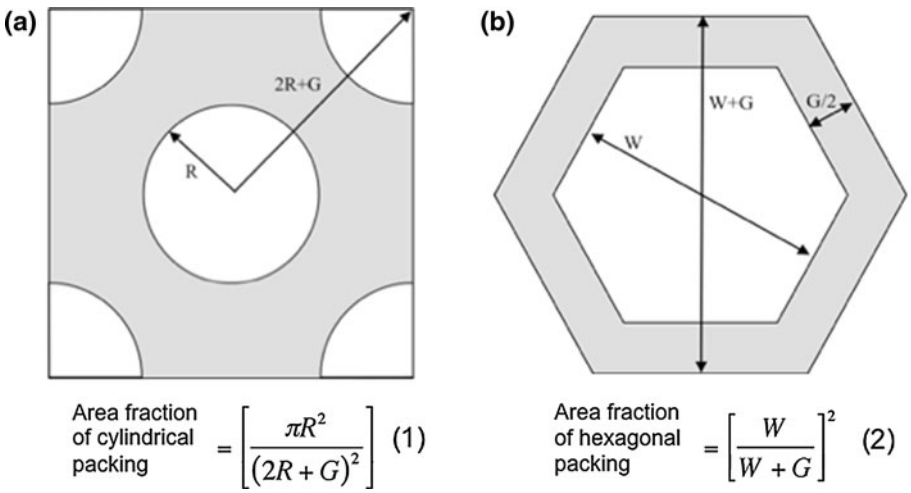

Fig. 3 Pore area figures and equations of **a** close-packed cylinders and **b** close-packed hexagons

cure for nerve damage. The approach is centered on the fabrication of scaffolds to enable bridging through the injury and re-establishing nerve continuity. The method reported in this work uses a technology that can precisely control scaffold microchannel size, separation between microchannels and maintain a high degree of ordering in the range of mm–cm both perpendicular and parallel to the direction of axon growth. The scaffolds are designed and fabricated such that axon growth is consistent with the native nervous system environment with regard to relative axonal position and density. Precision compartmentalization, small (tens of microns to hundreds of micron microchannels) separated by micron to 100 μm walls, in theory should enable the near restoration of original nerve pathways following a spinal cord injury. Our approach for achieving this scaffold technology involves a material patterning process that uses wet chemical etching to selectively remove polymer optical fibers while leaving the permissive axonal growth substrate, agarose hydrogel, intact. Selective etching of fiber-like mandrils has been used by other groups to fabricate microchannels in other permissive substrates such as poly(2-hydroxyethyl methacrylate), poly(lactic-co-glycolic acid), and poly(L-lactic acid) [23–30]. The scaffold patterning approach presented in this study differs from previous work in that it involves a technology to prepare highly ordered arrays of microchannels with the ability to precisely control the spacing and diameter of the microchannels in the tens to hundreds of micron range. The degree of ordering is a key feature in that it enables the fabrication of scaffolds with unprecedented microchannel volume of 80%.

Increasing the scaffold dimensions in the plane perpendicular to axon growth from millimeters to centimeters did require some modifications to previous study. As the dimensions perpendicular to longitudinal length increase beyond a few mm, it became increasingly difficult to selectively remove the PMMA cladding at the center of the MCFB templates. As the lateral dimension increased, the lack of convective solvent flow within the interstices of the fibers caused the PC etchant to reach its solubility limit, thus slowing the etch rates towards the center of the MCFB. This was mitigated by adding ACN to the PC etch bath. PMMA has a higher solubility in ACN, thus lateral etch rates can be increased compared to the pure PC etchant. However, PS also has a higher solubility in ACN, thus only 20 vol% was added to allow complete PMMA removal. Additionally, the use of ACN likely lowered the viscosity of the PC/ACN etch bath to further facilitate solvent convection within the interstices of the fibers. A related issue involved permeating the molten agarose hydrogel through the templates again as the dimensions perpendicular to the longitudinal direction increased. However, centrifuging the templates facilitated agarose hydrogel permeation to overcome this issue.

3.1 Cross sectional and depth analysis

Measurements for microchannel diameter and wall thickness for 25/200, 43/320, 54/172, 67/200, and 88/210 scaffolds are listed in Table 1 (the scaffold wall "W" and microchannel "MC" dimensions are reported as W/MC where the values are given in microns). For example, the 25/200 scaffolds consist of a mean wall thickness of 25 μm and a mean channel diameter of 200 μm. All of the scaffolds in this study group were prepared with PS fiber templates. One set of scaffolds (highlighted with an asterisk) was prepared with PMMA fibers that will be discussed in a subsequent section below. The scaffolds listed in Table 1 had overall cross-sections ranging from 20 to 100 mm^2 with 7.5 mm long microchannels. There were two reasons for selecting 7.5 mm long microchannels to compare the cross-sections of multiple scaffold configurations. First, 7.5 mm was, on the whole, the maximum microchannel length at which no significant disorder along the entire longitudinal length of the scaffolds was observed. By minimizing the amount of disorder, detailed statistical analyses could be conducted to characterize the linearity of the microchannels and walls. The ability to fabricate microchannels longer than 7.5 mm was investigated in a separate study in a subsequent section below. Secondly, 7.5 mm was selected because it demonstrates the ability to fabricate scaffolds with considerably longer microchannels compared to our previously reported work involving 2.0 mm long microchannels. The cross-sectional analyses of all the 7.5 mm long scaffolds demonstrate several key aspects and are described in detail below.

3.1.1 Etching and permeation of agarose hydrogel

The ability to completely etch or remove the PMMA cladding and permeate the agarose hydrogel between the fibers was demonstrated. This is evident from the cross-sectional images that show uniform channel and wall ordering through out the scaffolds, as discussed in greater detail below. The 43/320 scaffolds, in particular, were successfully fabricated with dimensions of 1 cm × 1 cm × 1 cm (Fig. 4), thus demonstrating a significant increase in lateral dimensions compared to our previous study. Scaffolds with these dimensions are also believed to represent a significant step towards achieving clinically relevant length scales.

3.1.2 Patterning process efficiency

For the most part, the fabrication process produces scaffolds that are near duplicates of the MCFB templates used to pattern them. The endcaps secure the fibers in place through out the etching and permeation steps to enable

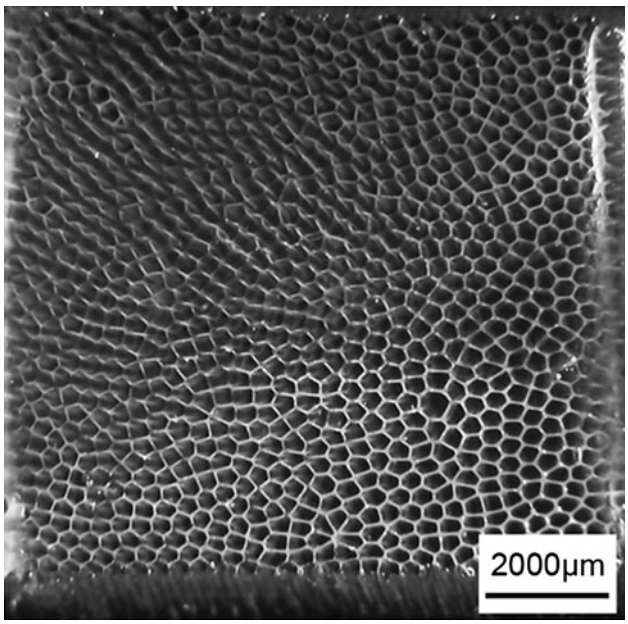

Fig. 4 Cross-section of 320 μm microchannel diameter, 43 μm wall thickness scaffold

highly ordered arrays of microchannels. The wall and microchannel diameter percent difference between the MCFB template dimensions and scaffold dimensions is plotted in Fig. 5. From Fig. 5, in most of the scaffolds prepared, the percentage difference between scaffold and template for both microchannel diameter and wall thickness is low. It is interesting to note that the dimensional percent difference between the 25/200, 43/320, and 54/172 scaffolds are significantly lower than the 67/200 and 88/210 scaffolds. This is most likely due to variances between MCFB batches. Additionally, differences in wall thickness and microchannel diameters at all depths for 67/200 and 88/210 samples, as seen in Table 1, are quite low, further indicating MCFB batch irregularities.

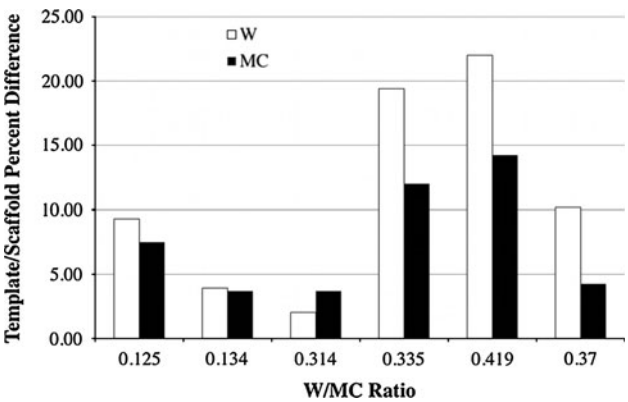

Fig. 5 Percent difference between MCFB template and scaffold dimensions of wall thickness (W) and microchannel diameter (MC). Percent difference for small W/MC ratios are relatively low, but increases with W/MC

3.1.3 Statistical microchannel depth analyses

Cross-sectional analyses were performed along the longitudinal axes of 7.5 mm long scaffolds to evaluate the microchannel and wall organization as a function of microchannel depth. Cross-sections were taken at 1, 3.75 and 6 mm intervals perpendicular to the longitudinal axis of the 7.5 mm long scaffolds as described in the experimental section above. For brevity, representative cross-sections from each scaffold are shown in Fig. 6. A summary of the cross-sectional data is presented in Table 1.

The cross-sectional analyses of the scaffolds with various W/MC ratios indicate several noticeable trends. First, the scaffold walls are continuous along the entire length of the microchannels. For the most part, the walls are consistent in thickness; however, they tend to be the thinnest at a microchannel depth of 3.75 mm in almost all cases. Moreover, the lower the W/MC ratio, the higher the degree of deflection at 3.75 mm depth compared to the average wall thicknesses at 1.0 and 6 mm depth (Fig. 7). For example, at a microchannel depth of 3.75 mm, the scaffolds with a W/MC ratio of 0.125 (25/200) have walls that are 26% thinner while the scaffolds with a W/MC ratio of 0.419 (88/210) are only 1% thinner. The reason for this is likely due to capillary forces that draw the fibers closer together during the agarose permeation and gelation processing steps. The closer the fibers are initially, the greater the capillary forces are. Since the fibers are constrained on their ends, the deflection is the greatest at the farthest point from the endcaps, i.e., in the middle. Second, the variation in microchannel diameter is, for the most part, negligible in all scaffolds at all depths. The high degree of microchannel diameter consistency demonstrates the efficacy of the MCFB patterning process. The fibers direct the solidification of the liquid precursor at the molecular scale, thus the microchannels are near replicas of the fibers used to pattern them. Third, the number of microchannels per unit volume should be maximized up to a certain point. That point is determined by the minimum microchannel diameter at which axonal extension is no longer sustainable. Support cells and vascularization are required in the microchannels, thus the microchannels must be above a critical diameter. Similarly, there are practical limits from a processing perspective. As the microchannel diameters decrease, and the targeted microchannel lengths remain the same, the aspect ratio of the patterning fibers increases.

In this study, the aspect ratios range from 23:1 to 43:1 for the 43/320 and 54/172 scaffolds, respectively. Typically, as the aspect ratio increases, the fibers are less linear especially toward the mid span as described above. Thus, if the targeted microchannel lengths are in the 1–2 cm range, there should be a lower limit to how small the microchannels can be. Nevertheless, this work reports the

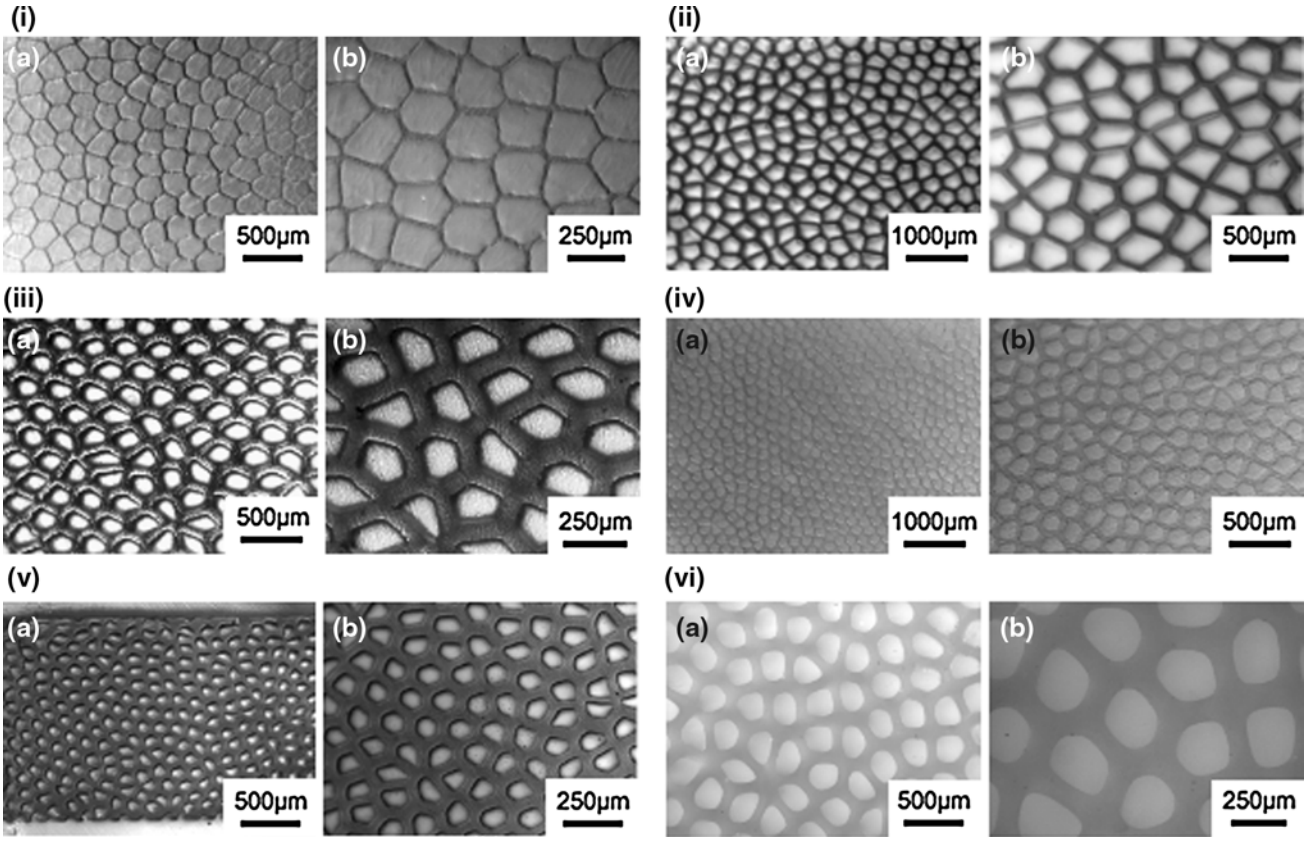

Fig. 6 Representative cross-sections of **i** 25/200, **ii** 43/320, **iii** 67/200, **iv** 54/172, **v** 88/210, and **vi** inverse 94/254

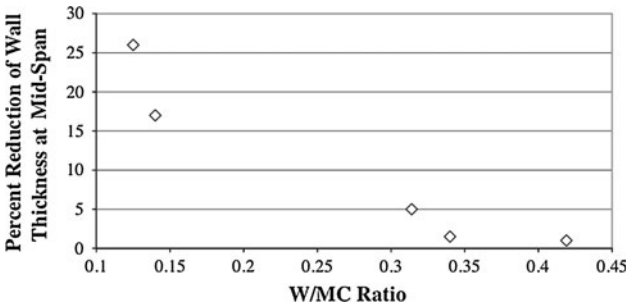

Fig. 7 As the W/MC ratio decreases, the degree of microchannel coalescence increases

successful fabrication of 172 micron diameter microchannels that are 7.5 mm long (43:1 aspect ratio) compared to our previous work that reported 200 micron diameter microchannels that are 2 mm long (10:1 aspect ratio) [15].

It is also interesting to note that the 67/200 scaffolds have a lower than expected wall thickness variance. This could be attributed to a subtle difference in the method used to fabricate the MCFB templates. Specifically, this set of MCFB templates may have been etched in a slightly cooler etch bath, which, apparently, produces less fiber distortion. This phenomenon became apparent toward the end of this work and will be incorporated into future study as it appears to further improve the precision of the patterning process.

A combination of smaller diameter microchannels and a relatively low W/MC ratios result in maximum of 28 microchannels per mm^2 of cross-sectional area for the 54/172 scaffolds. The other scaffolds in this study had combinations of microchannel diameters and W/MC ratios that typically resulted in scaffolds with 10–16 microchannels per mm^2 of cross-sectional area. As mentioned above, the number of microchannels per unit cross-sectional area should be optimized to provide adequate physical confinement to ensure linear axon extension through a lesion site while enabling the infusion of the necessary support cells into the scaffolds. The optimum microchannel diameter has not been determined at this time, but the scaffold fabrication process reported in this work can produce microchannels over an appropriate range to empirically determine the optimum microchannel diameter. Likewise, future work seeks to evaluate the effect of axonal extension based on scaffolds with microchannel diameters ranging from 10–200 μm.

The 25/200 scaffolds had the thinnest mean wall thickness of all the scaffolds in this study. However, it was found that the scaffolds having a small average wall thickness (25 μm) and a substantially higher standard

deviation (40% at 1 mm depth) created regions of the scaffold with walls too thin to withstand the rigors of implantation, as orally communicated by MH Tuszynski, PhD/MD (August 2009). In the past, the 88/210 scaffolds used for in vivo testing did not exhibit mechanical failures, which is the result of having consistently thicker walls. Attempts to overcome this thin wall issue involved increasing the weight percentage of agarose hydrogel to 4.5 wt% to provide scaffolds with higher strength, but regardless these scaffolds were unable to withstand fabrication loads. Thus, without additional reinforcement, it is postulated this W/MC ratio is unsuitable for in vivo experiments or until further improvements to the mechanical properties of agarose hydrogel can be made. Currently, however, the focus has been on increasing the microchannel volume, thus the 67/200 scaffolds are used in in vivo experiments. To date, numerous in vivo experiments have been conducted with the 67/200 scaffolds in which there have been few scaffolds that ruptured or collapsed during implantation or the course of the experiment. The results of this work will be included in a future publication.

3.1.4 Microchannel volume analysis

The effect of W/MC ratio on nerve guidance area is plotted in Fig. 8. The solid line and dashed lines represent the theoretical values calculated by Eq. 1 and 2 for hexagonally close-packed hexagons and cubic close-packed cylinders, respectively. The actual nerve guidance volume values were calculated as described above for the 25/200, 43/320, 54/172, 67/200, *94/254 and 88/210 scaffolds and compared to the theoretical predictions. Actual values were expected to fall between the range specified by the theoretical predictions. However, samples with 43/320 and 54/172 W/MC dimensions were significantly higher. Likewise, samples with W/MC dimensions of 88/210 and 25/200 were lower than expected. These results indicate microchannel packing arrangements unlike those predicted. It is hypothesized that the geometry of the microchannels with irregular shapes further increases the volume ratio of microchannels, resulting in microchannel porosity higher or lower than the predicted theoretical values. It is important to note that the ability to form highly ordered arrays of fibers or microchannels enables the fabrication of scaffolds with unprecedented microchannel volume. Our previous study [15] reported microchannel volumes in the 44% range using the 88/210 scaffolds. By reducing the scaffold W/MC ratio (Fig. 8) by a factor of about 3 microchannel volume increased to the 80% range. In other words, compared to our previous study, a doubling of regenerated axons could be achieved with W/MC ratios in the 0.14 range.

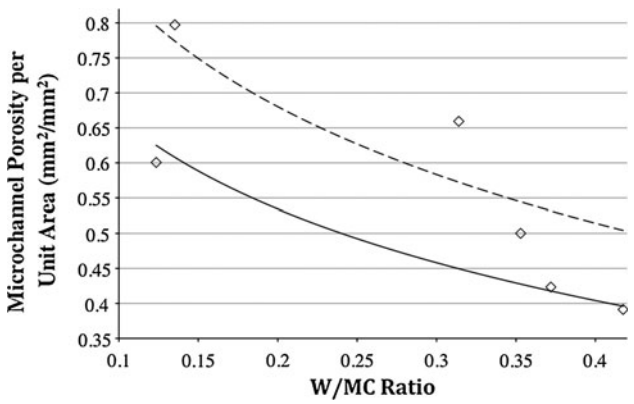

Fig. 8 Percent microchannel porosity compared to theoretical calculations of samples (from *left* to *right*) 25/200, 43/320, 54/172, 67/200, *94/254 and 88/210. The *solid line* represents the theoretical prediction using close-packed arrays of cylinders and the *dashed line* represents the theoretical prediction using close-packed arrays of hexagon pillars. (*inverse template)

3.1.5 Microchannel trajectory tracking

A cluster of microchannels was identified in a 54/172 scaffold and their trajectories were tracked through the length of the scaffold (Fig. 9). Typically, most microchannels form nominally arranged hexagonal arrays. In some cases a few clusters of microchannels deviate from a hexagonal arrangement and form a unique cluster such as the cluster of four microchannels highlighted in Fig. 9. The cluster identifies the same microchannels allowing their trajectories to be tracked along the entire length of the scaffold. The microchannels maintain the same position with consistently defined walls in each of the cross-sections demonstrating continuity from end to end.

3.2 Two centimeter scaffold fabrication

While the fabrication of scaffolds with discrete, ordered microchannels has been demonstrated at lengths approaching 1 cm, further refinement is required to achieve similar scaffolds that are 2 cm in length. Specifically, when 2 cm long scaffolds are prepared using MCFBs consisting of PS fibers and PMMA cladding, the microchannels deviate laterally significantly more along the length of the scaffold compared to those with 1 cm long dimensions. It is believed that the disorder occurs due to hydrophobic and capillary forces, as described previously. We hypothesized that achieving a higher degree of linearity beyond 1 cm could be achieved using an inverse template, i.e. PMMA fibers and PS cladding. The rationale for this stems from the fact that PMMA has a higher rigidity and is hydrophilic. Higher rigidity should result in a higher degree of microchannel linearity at longer microchannel lengths.

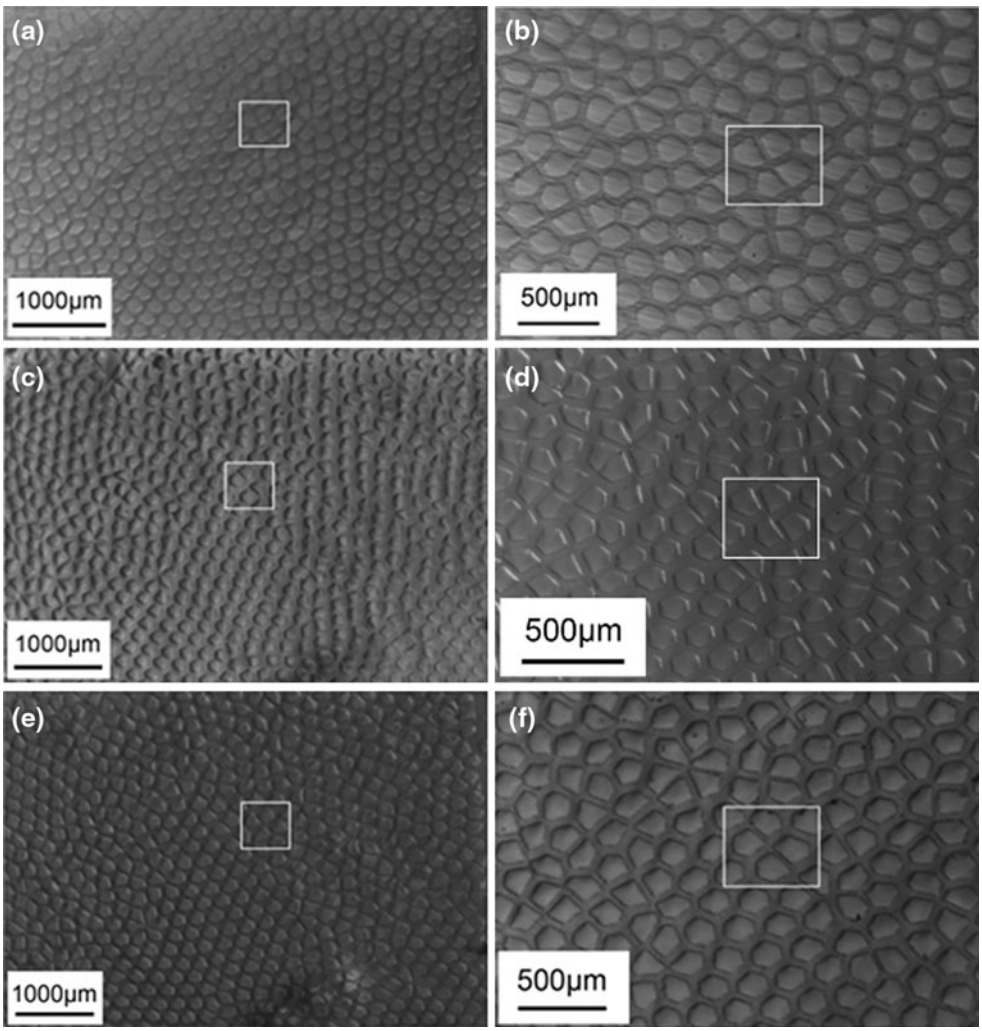

Fig. 9 The microchannel trajectory trace in a 54/172 scaffold demonstrates end-to-end continuity and linearity

Likewise, hydrophilic fibers should be beneficial in that they are more likely to be wetted by molten agarose hydrogel during fabrication, thus making fiber or microchannel coalescence less likely.

A study was conducted to compare scaffolds prepared from 2 cm long PS-fiber templates versus scaffolds prepared from 2 cm long inverse MCFB templates (Fig. 10). Figure 10 shows the side view of the PS (top) and PMMA (bottom) fiber MCFB templates before the molten agarose hydrogel was permeated. The figure also shows the cross-sections cut from the agarose hydrogel scaffolds made from the respective fiber templates at various depths along the length of the scaffold from one end to the middle of the scaffold. The microchannel organization at the middle of the scaffold (mid-span) is the key point of comparison. From this study, several points can be made. First, significant deviation in linearity is apparent in the PS-fiber template while the PMMA fibers maintain linearity. This is likely due to higher rigidity of PMMA compared to the PS fibers, thus exhibiting more linear microchannels. Secondly, the degree of microchannel organization at most depths of the scaffolds, especially at mid-span, appears to be significantly higher in the scaffold templated with the PMMA fibers. From this comparison, it is believed that the PMMA fiber templates are more likely to produce scaffolds with highly ordered, linear microchannels approaching clinical relevant length scales.

4 Conclusion

An approach for patterning nerve guidance scaffolds with unprecedented order, scale and microchannel volume was investigated. A wet etching technique involving polystyrene and poly(methyl methacrylate) multi-component fiber bundles was used to pattern, highly ordered, high aspect ratio microchannels in agarose hydrogel-based central and peripheral nerve scaffolds. Although the approach for

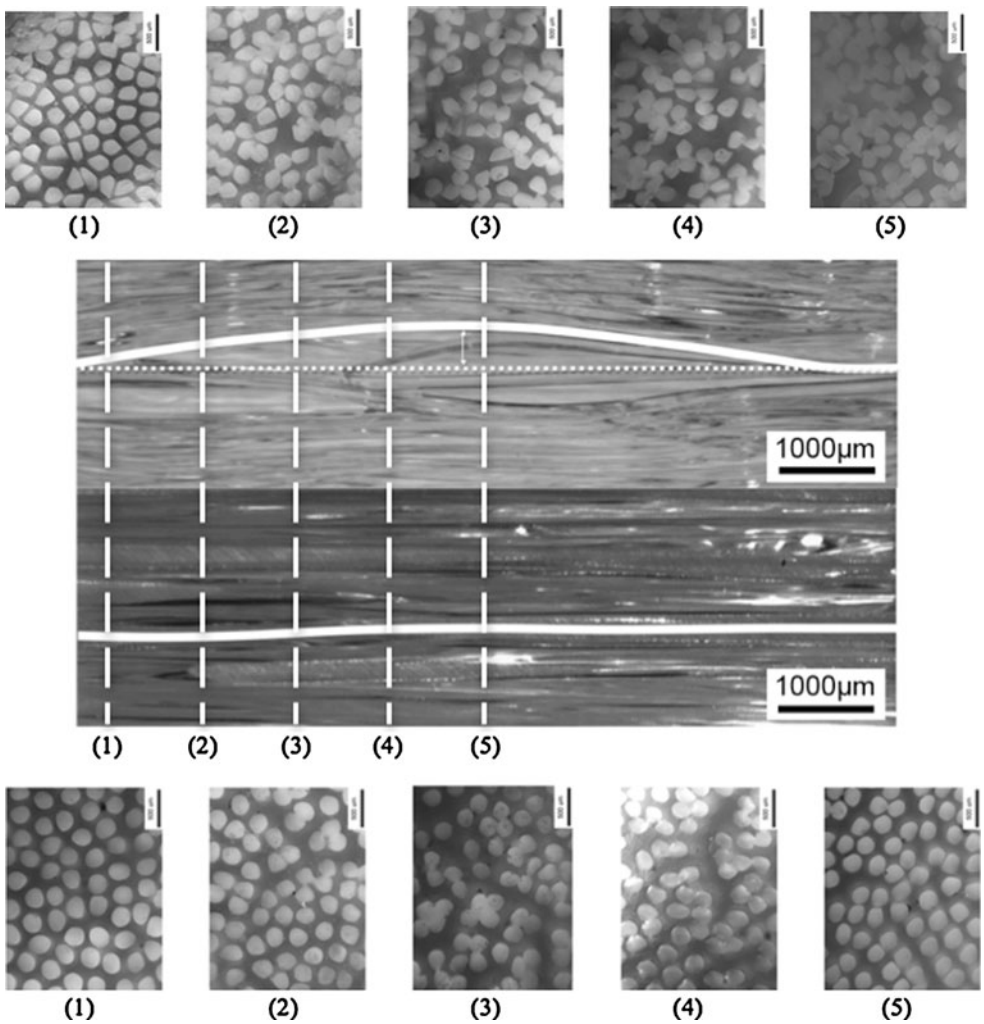

Fig. 10 Polystyrene fiber tracing along scaffold length (*Top*). Poly(methyl methacrylate) fiber tracing along scaffold length (*Bottom*). Both were taken at 8× magnification on scaffolds 2 cm in length

making smaller scale scaffolds was previously reported, this study focused on and demonstrated the scaling of scaffolds to clinically relevant length scales in the centimeter range. By using various polymer fiber configurations, scaffolds were fabricated with walls in the 27–94 micron range with microchannels in the 172–320 micron diameter range. The percentage of nerve guidance microchannel volume per unit volume of the scaffold was as high as 80%, which is believed to be the highest value reported for a multi-luminal nerve guidance scaffold. While microchannel organization was optimal when microchannel lengths were below 1, 2 cm long microchannels maintained reasonably ordered microchannels when using PMMA fiber templates instead of PS fiber templates. Present and future study focuses on further improving microchannel integrity in 2 cm long scaffolds as well as integrating drug delivery technology into the scaffolds walls to elute nerve growth factors.

Acknowledgments This study was supported by the Veterans Administration and the Christopher Reeve Paralysis Foundation. The authors would also like to thank Dr. Mark Tuszynski at the University of California, San Diego for his insightful interaction and assistance with characterizing the in vivo efficacy of the scaffolds described in this study.

References

1. Christopher Reeve Paralysis Foundation. One degree of separation: paralysis and spinal cord injury in the United States. Online. Christopher Reeve Paralysis Foundation; 2009. Available from URL: http://www.christopherreeve.org/site/c.mtKZKgMWKwG/b.5184239/k.58F3/One_Degree_of_Separation.htm.
2. Archibald SJ, Krarup C, Shefner J, Li ST, Madison RD. A collagen-based nerve guide conduit for peripheral nerve repair: an electrophysiological study of nerve regeneration in rodents and nonhuman primates. J Comp Neurol. 1991;306:685–96.
3. Liu BS. Fabrication and evaluation of a biodegradable proanthocyanidin-crosslinked gelatin conduit in peripheral nerve repair. J Biomed Mater Res. 2008;87A:1092–102.

4. Evans GRD, Brandt K, Widmer MS, Lu L, Meszlenyi RK, Gupta PK, et al. In vivo evaluation of poly(L-lactic acid) porous conduits for peripheral nerve regeneration. Biomaterials. 1999;20: 1109–15.
5. Matsumoto K, Ohnishi K, Kiyotani T, Sekine T, Ueda H, Nakamura T, et al. Peripheral nerve regeneration across an 80-mm gap bridged by a polyglycolic acid (PGA)-collagen tube filled with laminin-coated collagen fibers: a histological and electrophysiological evaluation of regenerated nerves. Brain Res. 2000;868:315–28.
6. Widmer M, Gupta P, Lu L, Meszlenyi R, Evans G, Brandt K, et al. Manufacture of porous biodegradable polymer conduits by an extrusion process for guided tissue regeneration. Biomaterials. 1998;19:1945–55.
7. Stokols S, Tuszynski MH. Freeze-dried agarose scaffolds with uniaxial microchannels stimulate and guide linear axonal growth following spinal cord injury. Biomaterials. 2006;27:443–51.
8. Martin BC, Minner EJ, Wiseman SL, Klank RL, Gilbert RJ. Agarose and methylcellulose hydrogel blends for nerve regeneration applications. J Neural Eng. 2008;5:221–31.
9. Sondell M, Lundborg G, Kanje M. Regeneration of the rat sciatic nerve into allografts made acellular through chemical extraction. Brain Res. 1998;795:44–54.
10. Crouzier T, McClendon T, Tosun Z, McFetridge PS. Inverted human umbilical arteries with tunable wall thicknesses for nerve regeneration. J Biomed Mater Res A. 2009;89A:818–28.
11. Wang KK, Costas PD, Bryan DJ, Jones DS, Seckel BR. Inside-out vein graft promotes improved nerve regeneration in rats. J Reconstruc Microsurg. 1993;14:608–18.
12. Heath C, Rutkowski G. The development of bioartificial nerve grafts for peripheral-nerve regeneration. Trends Biotechnol. 1998;16:163–8.
13. Ma PX, Zhang R. Microtubular architecture of biodegradable polymer scaffolds. J Biomed Mater Res. 2001;56:469–77.
14. Hadlock T, Elisseeff J, Langer R, Vacanti J, Cheney M. A tissue-engineered conduit for peripheral nerve repair. Arch Otolaryngol Head Neck Surg. 1998;124:1081–6.
15. Stokols S, Sakamoto J, Breckon C, Holt T, Weiss J, Tuszynski MH. Templated agarose scaffolds support linear axonal regeneration. Tissue Eng. 2006;12:2777–87.
16. Gros T, Sakamoto S, Blesch A, Havton LA, Tuszynski MH. Regeneration of long-tract axons through sites of spinal cord injury using templated agarose scaffolds. Biomaterials. 2010;31: 6719–29.
17. Lundborg G, Dahlin LB, Danielsen N, Gelberman RH, Longo FM, Powell HC, Varon S. Nerve regeneration in silicone chambers: influence of gap length and of distal stump components. Exp Neur. 1982;76:361–75.
18. Suzuki Y, Tanihara M, Ohnishi K, Suzuki K. Cat peripheral nerve regeneration across 50 mm gap repaired with a novel nerve guide composed of freeze-dried alginate gel. Neurosci Lett. 1999; 259:75–8.
19. Ansselin A, Fink T, Davey D. Peripheral nerve regeneration through nerve guides seeded with adult Schwann cells. Neuropath Applied Neurobio. 1997;23:387–98.
20. Kiyotani T, Teramachi M, Takimoto Y. Nerve regeneration across a 25-mm gap bridged by a polyglycolic acid-collagen tube: a histological and electrophysiological evaluation of nerves. Brain Res. 1996;740:66–74.
21. Sinis N, Schaller H, Schulte-Eversum C, Schlosshauer B, Doser M, Dietz K, Rosner H, Muller H, Haerle M. Nerve regeneration across a 2-cm gap in the rat median nerve using a resorbable nerve conduit filled with Schwann Cells. J Neurosurg. 2005;103:1067–76.
22. Mehrotra S, Lynam D, Maloney R, Pawelec K, Tuszynski MH, Lee I, Chan C, Sakamoto J. Time controlled protein release by layer-by-layer assembled multilayer functionalized agarose hydrogels. Adv Func Mat. 2009;20:247–58.
23. Flynn L, Dalton PD, Shoichet MS. Fiber templating of poly(2-hydroxyethyl methacrylate) for neural tissue engineering. Biomaterials. 2003;24:4265–72.
24. Rodríguez F, Gomez N, Perego G, Navarro X. Highly permeable polylactide-caprolactone nerve guides enhance peripheral nerve regeneration through long gaps. Biomaterials. 1999;20:1489–500.
25. Plikk P, Malbert S, Albertsson AC. Design of resorbable porous tubular copolyester scaffolds for use in nerve regeneration. Biomacromolecules. 2009;10:1259–64.
26. Moore M, Friedman J, Lewellyn E. Multiple-microchannel scaffolds to promote spinal cord axon regeneration. Biomaterials. 2006;27:419–29.
27. Bender M, Bennett J, Waddell R, Doctor J, Marra K. Multi-channeled biodegradable polymer/CultiSpher composite nerve guides. Biomaterials. 2004;25:1269–78.
28. Huang, et al. Manufacture of porous polymer nerve conduits through a lyophilizing and wire-heating process. J Biomed Mater Res: Appl Biomater. 2005;74B:659–64.
29. Wong D, Leveque JC, Brumblay H, Krebsbach P, Hollister S, LaMarca F. Macro-architectures in spinal cord scaffold implants influence regeneration. J Neurotrauma. 2008;25:1027–37.
30. Ghosh S, Viana J, Reis R, Mano J. Development of porous lamellar poly(L-lactic acid) scaffolds by conventional injection molding process. Acta Biomater. 2008;4:887–96.